Applied Catalysis B: Environmental 236 (2018) 76–87

Contents lists available at ScienceDirect

Applied Catalysis B: Environmental

journal homepage: www.elsevier.com/locate/apcatb

Flowing nitrogen atmosphere induced rich oxygen vacancies overspread the surface of TiO_2/kaolinite composite for enhanced photocatalytic activity within broad radiation spectrum

Chunquan Li[a,b], Zhiming Sun[a,*], Ankang Song[a], Xiongbo Dong[a], Shuilin Zheng[a,*], Dionysios D. Dionysiou[b,*]

[a] School of Chemical and Environmental Engineering, China University of Mining and Technology (Beijing), Beijing 100083, PR China
[b] Environmental Engineering and Science Program, Department of Chemical and Environmental Engineering (DCEE), University of Cincinnati, Cincinnati, OH 45221-0012, USA

ARTICLE INFO

Keywords:
TiO_2
Kaolinite
Ciprofloxacin
Formaldehyde
Oxygen vacancy

ABSTRACT

Natural minerals are generally accepted as one of the most suitable carriers to support TiO_2 in photocatalytic and other applications because of their abundance, low cost, large surface area, and easy recyclability. Hence, in this work, a novel 0D/2D TiO_2/kaolinite composite endowed with presence of oxygen vacancies and surface defect sites was synthesized through a mild sol-gel method combining with nitrogen induction. Ciprofloxacin (CIP) was taken as the main target organic pollutant to study the photocatalytic performance of the synthesized catalyst. The results showed that the nitrogen treated TiO_2/kaolinite composite exhibited improving degradation performance for adsorption-photocatalytic elimination of CIP within broad radiation spectrum (200–800 nm). The synthesized composite exhibited enhanced reaction rate constant which is nearly 7.00, 2.54 and 3.13 times higher than that of bare TiO_2 treated with air under UV, solar, and visible light, respectively. Moreover, the newly prepared composite also exhibited significant enhancement towards the removal of formaldehyde under both UV and visible light. Radical scavenger experiments and ESR results indicated that holes should be the main oxidizing species within broad spectrum in the degradation system. The enhanced activity of nitrogen treated composite is mainly attributed to the induced oxygen vacancies as well as the intimate interface contact between TiO_2 and kaolinite, resulting in smaller grain size, higher light absorption ability, and faster carrier separation efficiency. It is expected that this high-efficiency composite photocatalyst based on natural minerals will be a promising candidate for the elimination of pharmaceutical and personal care products and volatile organic compounds within broad radiation spectrum.

1. Introduction

During the past decades, due to the extensive use of pharmaceutical and personal care products (PPCPs) in the fields like industry, medicine, aquaculture and livestock farming [1], different PPCPs pollutants are gradually becoming ubiquitous and difficult to be removed by conventional wastewater treatment processes. Environmental impacts such as frequent occurrence, recalcitrant properties and high-toxicity to humans and aquatic life of several of these compounds are gradually becoming more and more serious [2]. Air quality issues have also become of primary importance as a consequence of poor air quality in many areas and growing awareness around the world. Volatile organic compounds (VOCs) derived from outdoor sources (painting and printing industries, chemical industries, etc.) or indoor sources (formaldehyde, toluene, dioxins, etc.) pose hazardous effect to the environment and human health [3,4]. Considering the potential toxicity, mutagenicity and carcinogenicity of such contaminants of emerging concern, it is of high priority to minimize these adverse effects by using various treatment technologies. Several physical, chemical and biological methods have been extensively investigated for the effective removal of PPCPs and VOCs; however, some of these processes have certain drawbacks such as low-efficiency, generation of secondary pollution, high cost, etc. Thus technologies based on TiO_2 photocatalytic materials endowed with low-toxicity, photoactivity under solar light, chemical stability and potential for recyclability, are viewed as promising alternative environmental remediation solutions in the future [5].

Nevertheless, it is widely accepted that pure TiO_2 usually has some

* Corresponding authors.
E-mail addresses: zhimingsun@cumtb.edu.cn (Z. Sun), zhengsl@cumtb.edu.cn (S. Zheng), dionysios.d.dionysiou@uc.edu (D.D. Dionysiou).

https://doi.org/10.1016/j.apcatb.2018.04.083
Received 4 March 2018; Received in revised form 28 April 2018; Accepted 30 April 2018
Available online 02 May 2018
0926-3373/ Published by Elsevier B.V.

drawbacks which severely influenced its industrial applications. These include limited spectral response and low photocatalytic efficiency (i.e., conversion of photons to reactive oxygen species such as OH) due to high electron-hole recombination. The natural solar light is composed of ca. 5% UV light, 45% visible light and about 50% near infrared (NIR) light [6]. Thus in order to expand the optical absorption range and capability of TiO_2 under sunlight, persistent efforts have been made to alter the chemical structure composition of TiO_2 by adding specific metal or nonmetal ions, constructing heterojunctions, and depositing noble metals which could effectively utilize photons and regulate the transfer pathways of photo-generated carriers [7–10]. All of these methods could expand the absorption spectrum range of TiO_2 to some extent and thus improve its solar photocatalytic performance [11]. Among these modification strategies, doping of TiO_2 with nonmetallic elements, especially nitrogen, can achieve significant optical absorbance under solar radiation due to the mixing of O 2p states with p states of N [12]. However, the nitrogen-doped TiO_2 absorption ability in the visible and infrared regions remains insufficient so far due to the restriction of superficial and internal structure composition. It is worth to mention that self-doping has demonstrated to be an effective way to adjust band structure, which could produce Ti^{3+} or Ti^{2+} species in TiO_2 as reported in recent studies [13–15]. Lattice disorder at the surface would be generated resulting in enhanced visible and infrared absorption [16]. The newly generated energy states can effectively contribute to the optical excitation and relaxation. Furthermore, surface oxygen vacancies with typical defect states can greatly restrict the charge carriers' recombination and promote the transfer and migration of the trapped electron-hole carriers to the adsorbents as well [17].

In addition, different kinds of natural minerals have been used to synthesize high-efficiency macro-micro (adsorption-photocatalytic) composite materials in the past decades [18–20]. Excellent degradation performance is usually obtained compared with pure TiO_2 due to the larger adsorption capacity, higher catalytic activity, and improved photo-induced carriers' separation efficiency. It is anticipated that better recyclability and stability will also be achieved through this process considering the size, dimension and properties of minerals. Kaolinite, as a two-dimensional layered aluminosilicate, endowed with thermal and chemical stability, high adsorption capacity, low cost, abundance and easy recycling [21], is a great candidate to use as material to develop 0D/2D structures for the highly photocatalytic degradation of environmental contaminants in aqueous and gaseous system.

In this work, a typical 0D/2D structure was designed and prepared through a mild sol-gel method. Nitrogen atmosphere was first applied to induce the TiO_2/kaolinite composite to generate surface oxygen vacancies and defect sites, which effectively tailor-design the optical, structural, dissociative adsorption, electronic and reductive properties of the composite. Ciprofloxacin (CIP) and formaldehyde were employed as representative PPCP and VOC, respectively, and the photocatalytic activities as well as the underlying mechanisms were also explored.

2. Experimental

2.1. Materials and reagents

The purified kaolinite utilized in our work was obtained from Suzhou City, China. Hydrochloric acid (HCl, ≥36.5%) was purchased from Sinopharm Chemical Reagent Co., Ltd (Beijing, China). Maya Reagent Co. (Zhejiang, China) provided the tetrabutyl titanate ($C_{16}H_{36}O_4Ti$, TBOT). The 5,5′-dimethyl-1-pirroline-*N*-oxide (DMPO) was obtained from Sigma Chemical Co. Ciprofloxacin was bought from Aladdin Industrial Corporation. Acetic acid (CH_3COOH), ethanol (C_2H_5OH), methanol (CH_3OH) and some other chemicals used in our study were bought from Beijing Reagent Co. (Beijing, China). The chemicals were all analytical reagent grade (≥99.7%) and all our experimental procedures used deionized water (resistivity ≥9.95 MΩ cm).

2.2. Catalyst synthesis

In this study, we used a mild sol-gel method to synthesize the nitrogen treated TiO_2/kaolinite composite. The preparation procedures were conducted as follows: In the first step, 1.0 g kaolinite was placed into the reaction beaker, then specific amounts ethanol and acetic acid were added as well; a magnetic stirring device was used to disperse the mixture with a constant temperature of 25 °C. After 30 min, 3 mL of tetrabutyl titanate (TBOT) were added into the suspensions drop by drop. In the following step, stirring was further continued for around 30 min, and then a peristaltic pump was used to enable the drop wise addition of a solution of water and ethanol (pH = 2, volume ratio = 1:1) into the suspensions. Next, 12 h stirring was continued for the obtained mixture. After that, an oven with 80 °C was used to dry the gel product. Finally, a tube furnace was employed to calcine the samples under air and N_2 atmosphere at different temperatures for 2 h, and both of heating ramp rate and cooling rate were set as 5 °C/min. The gas flow rate was controlled at 50 mL/min during the entire calcination process. Single TiO_2 was also synthesized by using the same method in the absence of kaolinite. The synthesis strategy is illustrated in Scheme 1.

2.3. Equipment and characterizations

The crystalline properties of the synthesized composites were tested by a D8 X-ray diffractometer (Bruker, Germany). The range of 2θ was set from 5° to 80° and the scanning speed was 4°/min. Scherrer's formula ($D = 0.89\,\lambda/\beta\cos\theta$) was used to calculate the average crystallite sizes of TiO_2. The lattice strain induced in TiO_2 powders, which was mainly caused by crystal distortion and imperfection, was calculated by using the following formula: $\varepsilon = \beta/4\tan\theta$ [22]. As for the SEM images and EDS patterns, an S-4800 (Hitachi, Japan) scanning electron microscopy (FESEM) was used in this work. Transmission electron microscopy and high resolution transmission electron microscopy images were obtained by using the Tecnai G2 F20 Transmission Electron Microscope which was operated at 200 kV. A Hitachi U-3010 spectrophotometer was used to present the UV–vis absorption spectroscopy. Infrared spectra were measured on a Nicolet 6700 FTIR spectrometer by using KBr plates. The Raman spectra were analyzed through a RENISHAW INVIA spectrometer with a CCD detector using a green 633 nm laser. The BET specific surface areas were measured using a JW-BK nitrogen adsorption apparatus (JWGB Sci. &Tech, Beijing) at low temperature (77 K). X-ray photoelectron spectrometer (XPS) provided by Thermo escalab 250Xi was utilized to conduct X-ray photoelectron spectroscopy measurement. The peak positions of the elements were calibrated by C 1s (284.8 eV). The electron spin resonance (ESR) was also used to detect the reactive species during the photocatalytic degradation process; radical signals were trapped by DMPO in water or CH_3OH and detected by the JEOL FA-200 spectrometer. Photoluminescence spectra (PL) of the composites were measured on the FLS920 life and steady state spectrometer (Edinburgh Instruments Ltd.), and the excitation wavelength was set as 350 nm. The electrochemical impedance spectroscopy (EIS), photocurrent (i–t), volt-ampere characteristics (I–V) and Mott-Schottky analysis were conducted on a CHI-660B electrochemical analyzer.

2.4. Ciprofloxacin degradation test

The photocatalytic activity of as-synthesized TiO_2/kaolinite composites calcined under different gas atmosphere were investigated via the degradation of ciprofloxacin (CIP) using a PL-03 photocatalytic reaction apparatus (Beijing Pulinsaisi plant, China). The degradation kinetic reactions of the synthesized composites illuminated under different conditions were all investigated using UV, solar or visible light. The corresponding light sources were a 300 W mercury lamp, a Xenon lamp (average light intensity 50 mW/cm^2) and a Xenon lamp equipped

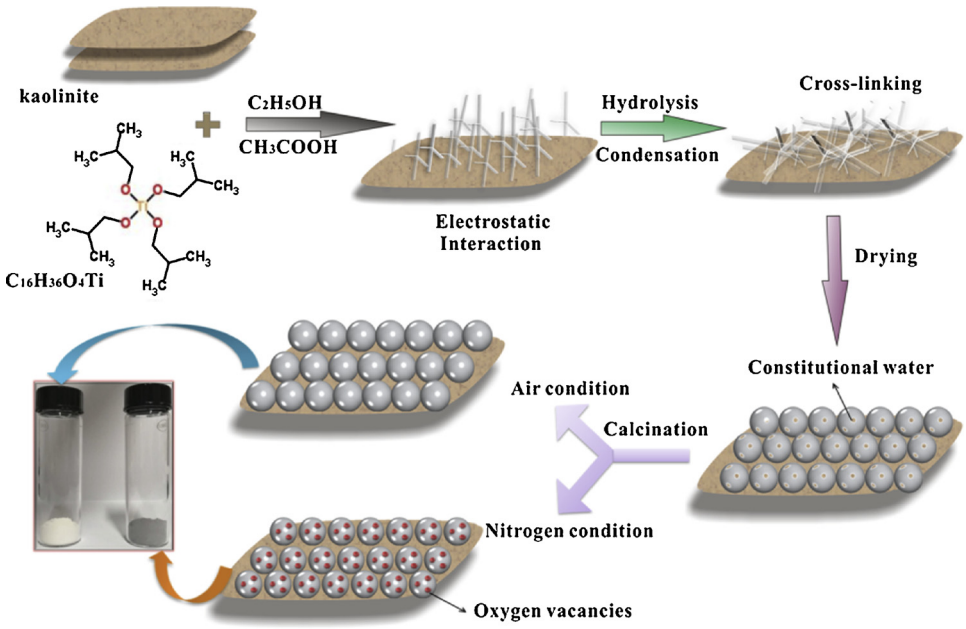

Scheme 1. The preparation strategy for the nitrogen treated TiO_2/kaolinite composite.

with a 400 nm cut-off filter (average light intensity 90 mW/cm^2), respectively. When conducting the experiments, 0.1 g of the as-synthesized catalysts was first dispersed in standard CIP (10 mg L^{-1}, 100 mL) through ultrasonic treatment, and then transferred into the cylindrical reactor with continuous magnetic stirring. Before illumination, dark reactions were carried out to reach the equilibrium of adsorption-desorption. At predetermined specific time interval, 2 mL of suspension was absorbed and separated through centrifugation with a rotation rate of 8000 rpm for 5 min, then filtered through the membrane filter (0.45 μm). UV–vis spectrophotometer (UV-6000s, Shanghai Metash) was used to evaluate the concentration of CIP through measuring the absorbance at 278 nm. Comparative experiments were also conducted by using pure TiO_2 as references. The CIP degradation and radical scavenger experiments were conducted in parallel.

2.5. Formaldehyde degradation experiments

In this study, a 250 L photocatalytic reactor was utilized to measure the formaldehyde degradation performance of the synthesized samples (Hunan Huasi, China) similar to our previous report [23]. The schematic diagram of the device is presented in Scheme 2. When conducting experiments, different samples (1.0 g) were uniformly spread on a glass plate surface (50 cm × 50 cm) by adding water first. After drying in the oven, coated plates were placed on the lifting platform within the reactor at room temperature and 60% relative humidity. Then the formaldehyde solution was injected into the reactor through a silicone rubber septum after sealing the reactor. In order to make the formaldehyde solution evaporate rapidly, a heating device was used at the injection port. Meanwhile, compressed air was introduced to vaporize the formaldehyde. Before illumination, the experiments were performed in the dark condition for 10 h. Experiments were carried out using UV light sources (16 W) or fluorescent lamps (28 W). The irradiation time was controlled at 120 min and 10 h, respectively. Formaldehyde concentration was measured using the spectrophotometric method based on China National Standard (GB/T 18204.26-2000). Twenty liters gas after reaction was collected through the atmospheric sampler, so that the gaseous reaction products could well dissolve into the as-prepared absorbing liquid. Then a purple compound would be formed because the non-degraded formaldehyde can react with 4-amino-3-hydrazino-1, 2, 4-triazol-5-thiol under alkaline environment by using the potassium periodate. Metash UV–vis spectrophotometer (Shanghai, China) was used to determine the concentration by measuring the absorbance at 550 nm. The initial theoretical concentration of HCHO was calculated as 1.920 ± 0.05 mg/m^3. The final removal rates were determined according to the variation of formaldehyde concentration before and after reaction.

2.6. Photoelectrochemical measurement

The photoelectrochemical properties of the TiO_2/kaolinite composites were also investigated in this study. The working electrode preparation procedures were as follows: 10 mg photocatalysts and 1 mL ethanol were well mixed and ultrasonicated for 15 min. Then, the resulting suspensions were dropped onto the ITO slices (2 cm × 1 cm). After air drying, the samples were dried for 4 h at 80 °C in an oven. A three-electrode system was established through using the reference electrode (Ag/AgCl), counter electrode (Pt wire), and working electrode (the as-prepared samples). During the testing, the light source was a 500 W Xe lamp. The photocurrent (i–t), electrochemical impedance spectroscopy (EIS) analysis, the volt-ampere characteristics (I–V) and the Mott-Schottky analysis were all performed in Na_2SO_4 aqueous solution (0.1 M) [24].

3. Results and discussion

The crystallographic structures of TiO_2/kaolinite composites with different calcination temperature under nitrogen and air atmosphere were tested by X-ray diffraction measurement as illustrated in Figs. 1, S1 and S2. It is clear that the pure kaolinite has a high purity and no obvious impurity peaks were observed (Fig. S1). The XRD pattern of kaolinite clearly displayed (001), (020), (002), (200) and (240) lattice planes at 12.28°, 19.87°, 24.88°, 35.97° and 55.04°, respectively, which was well corresponded to the standard kaolinite pattern (JCPDS No. 78-1996). The characteristic peaks of TiO_2 at around 25.3°, 37.8°, 48.1°, 53.9°, 55.1° and 62.7° were well corresponding to the crystal planes array of anatase TiO_2 (Fig. 1(a and b)). However, no distinct characteristic peaks of kaolinite were exhibited after calcination in TiO_2/kaolinite composite patterns, which could be ascribed to the stacking loss within the kaolinite layers and the completion of dehydroxylation reaction during this period [25]. From 500 °C to 850 °C, the kaolinite

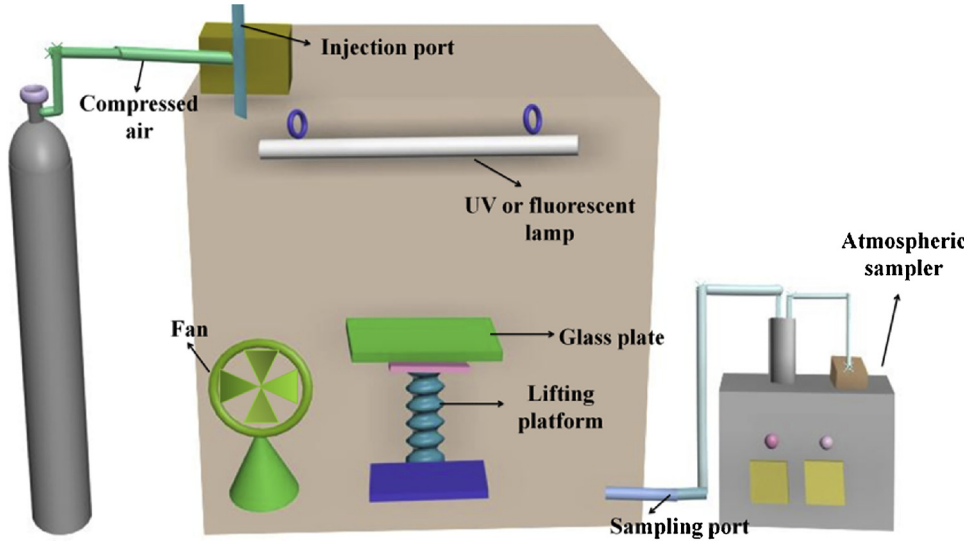

Scheme 2. The diagram of the device for the photocatalytic degradation of formaldehyde.

was presented in the form of amorphous metakaolinite, thus no obvious peaks were displayed in the figures. With increasing the calcination temperature, the enhancement of crystallinity were generated as seen from the (101) peak change of TiO_2 in the composite. In comparison with TiO_2 under air condition, the TiO_2 characteristic peaks in the TiO_2/kaolinite composite produced a pronounced broadening under nitrogen condition, indicating severe lattice distortion was generated in the nitrogen calcination process. This might be further verified from Fig. 1(d), the lattice strain variance demonstrated the significant impact of nitrogen atmosphere. It is well-known that surface imperfection and crystal distortion would be beneficial for the efficient transfer and separation of the photo-generated carriers [17,26]. The average grain

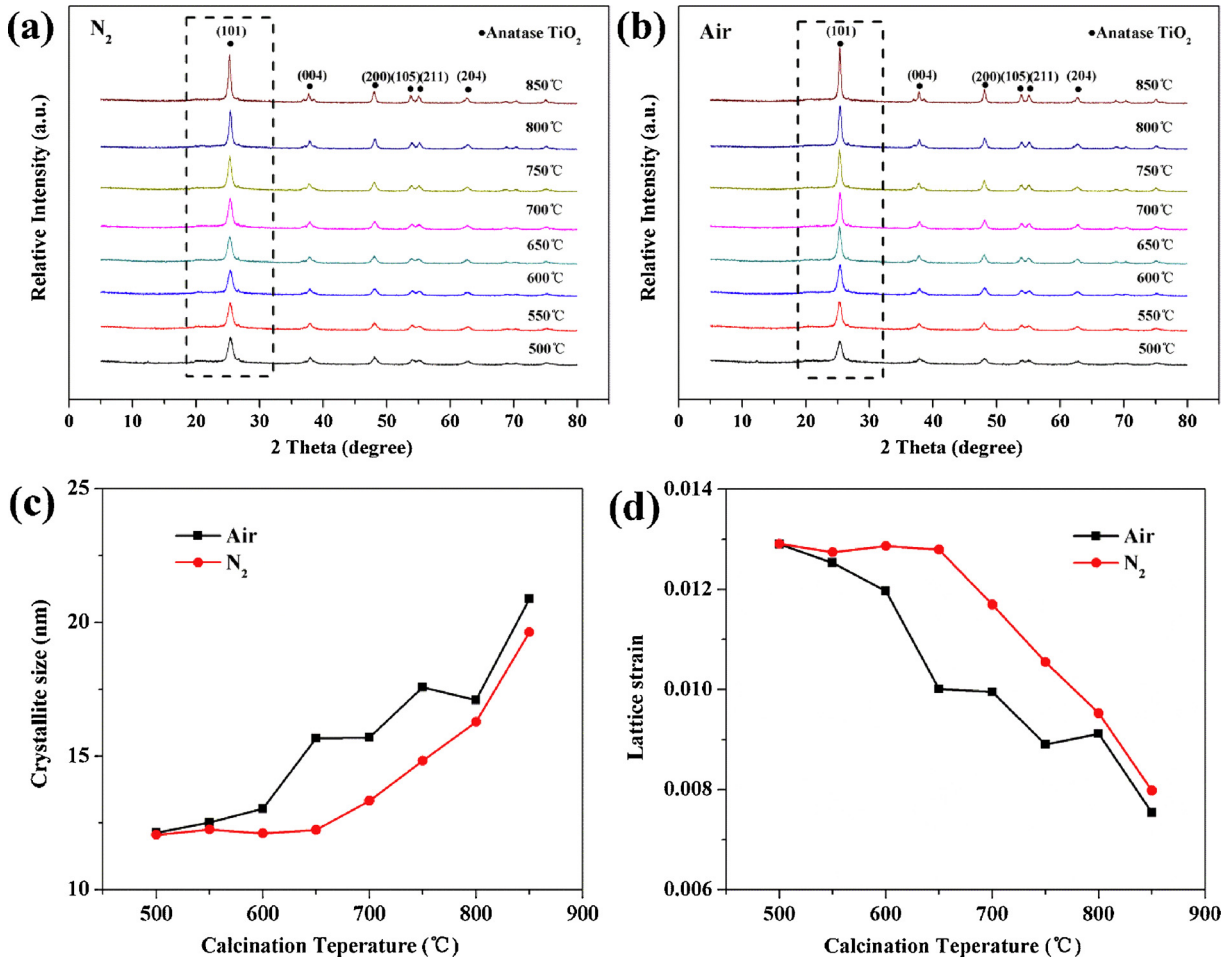

Fig. 1. (a and b) XRD spectra of TiO_2/kaolinite composites at different calcination temperature under nitrogen and air atmosphere, (c and d) The varieties of TiO_2 crystallite size (c) and lattice strain of TiO_2 (d) in the TiO_2/kaolinite composite at different calcination temperature under nitrogen and air atmosphere.

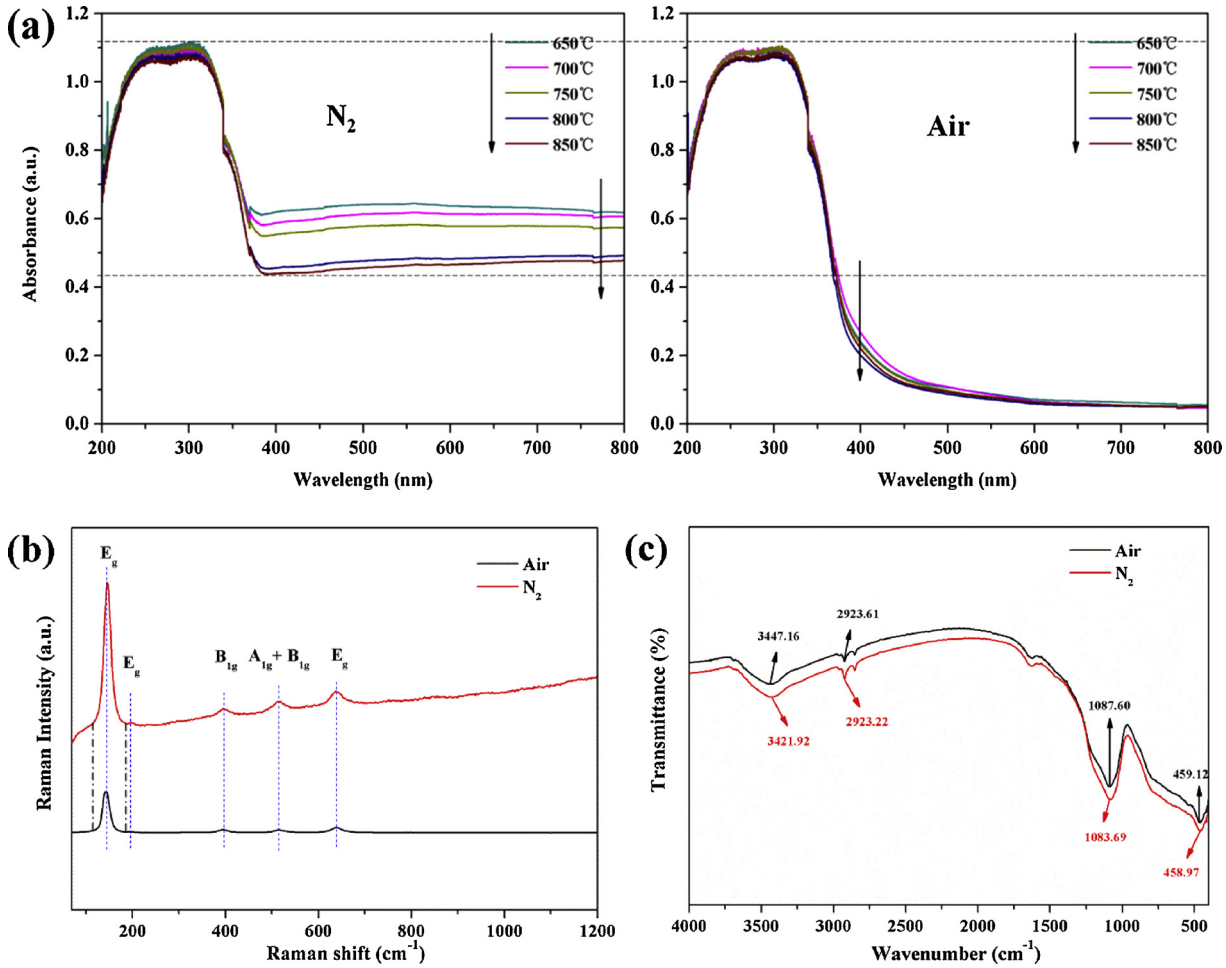

Fig. 2. (a) UV–vis DRS spectra for TiO_2/kaolinite composites at different calcination temperature under air and nitrogen atmosphere, (b and c) Raman and FTIR spectra of TiO_2/kaolinite composite under air and nitrogen atmosphere (800 ℃).

sizes of TiO_2 in the composite were also calculated and displayed in Fig. 1(c) based on Debye-Scherrer formula, suggesting the nitrogen condition could effectively decrease the crystalline sizes of the loaded TiO_2 nanoparticles. It is generally accepted that smaller grain size results in enhancement of photocatalytic activity [10].

To further examine the effect of nitrogen atmosphere towards the TiO_2/kaolinite composites, UV–vis DRS, Raman and FTIR analyses were performed (Fig. 2). As seen from Fig. 2(a), TiO_2/kaolinite composite with nitrogen atmosphere exhibited higher absorption ability under both UV light and visible light irradiation. The visible light absorption of TiO_2/kaolinite composite gradually decreased with increasing the calcination temperature, this because high temperature might induce grain size to increase and then cause the reduction of catalytic property [27]. Treatment under nitrogen which results in enhancement of light absorption plays a vital role in the photocatalytic reaction process since more photons will be absorbed and utilized within a unit time. Based on the degradation results under different calcination temperatures, the samples with calcination temperature of 800 ℃ were employed to carry out further characterization and research (Figs. S3 and S4). Fig. 2(b) is the Raman spectra of TiO_2/kaolinite composite under nitrogen and air condition. Six Raman active phonons are shown in $3E_g$ (144, 196 and 639 cm^{-1}), $2B_{1g}$ (397 and 519 cm^{-1}), and $1A_{1g}$ (513 cm^{-1}). Slight red shift as well as apparent enhancement and broadening of characteristic peaks were generated under nitrogen condition; this can be ascribed to the intrinsic defects of TiO_2 induced from the oxygen vacancies and deficiencies under nitrogen atmosphere [28]. It is known that finite grain size (< 10 nm) or defects inducing shorten correlation length result in phonon confinement effects. Moreover, the phonon confinement under nitrogen atmosphere explained the baseline irregularities [29]. FTIR analysis showed strong and wide peaks at around 3400–3450 cm^{-1} and 2920 cm^{-1}, which are caused by the stretching vibration of internal water molecules and surface hydroxyl groups. A significant peak at around 1085 cm^{-1} was derived from the Si—O and Al—O stretching vibration. The peak at approximate 460 cm^{-1} absorption band was attributed to Ti—O vibration absorption [30]. Red shift was produced as well because of the removal of oxygen lattice and the formation of Ti^{3+} sites on the reduced TiO_2 under nitrogen atmosphere [31].

Fig. 3 is the SEM images and EDS analysis results of TiO_2/kaolinite composites under nitrogen and air atmosphere. Three representative regions (A– C) were chosen to demonstrate the surface element composition of the synthesized composite under different atmosphere. Through the comparison, it is determined that the sample under nitrogen condition has a much higher O/Ti ratio than the sample under air condition. This is because nitrogen atmosphere can lead to the generation of internal lattice oxygen vacancies, and then the internal oxygen would diffuse and enrich on the surface of TiO_2/kaolinite composite [14,32]. It is also worth to mention that the relative content of Ti at low energy had an evident increase under nitrogen condition, which can be attributed to the generation and evolution of Ti^{3+} species [11]. Alberto Naldoni and his co-workers also proved that oxygen-poor environment or oxygen-depleted condition (H_2 or vacuum) was responsible for the change of lattice arrangement and composition which would result in the lattice distortion [13].

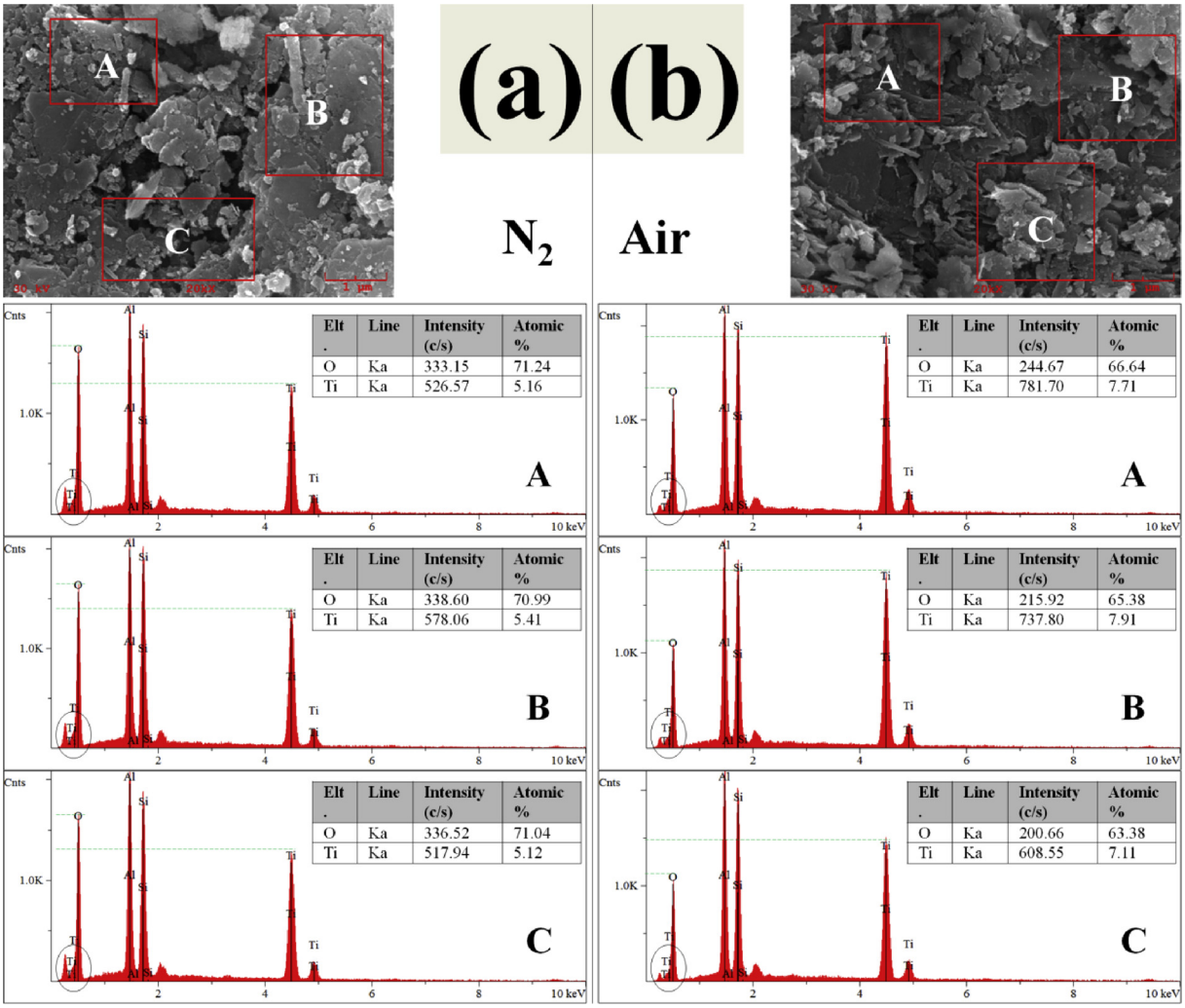

Fig. 3. (a and b) SEM images and EDS results (three regions, A– C) of TiO_2/kaolinite composites under nitrogen and air atmosphere (800 °C).

HRTEM and SAED were conducted in this work to further explore the effect of atmosphere on the morphology and crystallinity of the synthesized composite (Fig. 4). As exhibited in Fig. 4(a) and (g), nano TiO_2 particles were uniformly and densely distributed on the surface of kaolinite. Significant particle aggregation and agglomeration were inhibited due to the presence of natural layered kaolinite. Lower crystallite size was obtained compared with pure TiO_2 [33]. Besides, it is noticed that both TiO_2/kaolinite composites under nitrogen and air condition were well crystallized with the lattice spacing of 0.35 nm which was corresponded to the (101) plane of anatase TiO_2. However, in comparison to TiO_2/kaolinite composite under air condition, an interfacial angle of 82° was observed between the (101) and (011) atomic planes for the sample prepared under nitrogen atmosphere, which illustrated the crystal facet was exposed through the nitrogen treatment [34]. {111} facet has higher surface energy compared to other facets due to a large percentage of uncoordinated Ti and O atoms. These atoms could facilitate the formation of oxygen vacancies and promote the photocatalytic activity by acting as active sites in the photoreaction [35]. In addition, the SAED ring diffraction patterns under nitrogen and air condition with marked Miller indices of anatase TiO_2 are also given as displayed in Fig. 4(e, f) and (k, l). The typical 6-fold symmetric diffraction rings could be indexed with anatase TiO_2 (101), (004), (200), (105), (211) and (204) [36]. The ring pattern confirmed that the TiO_2/kaolinite composite is poly-crystalline, which might promote the enhancement of photocatalytic activity [36].

The nitrogen adsorption-desorption isotherm curves under nitrogen and air condition are displayed in Fig. 5(a). A typical H3 hysteresis loop as well as a type IV adsorption branch indicated the mesoporous characteristic structure. Combing with the results of BJH pore size distribution and *t-plot* (Fig. 5(a and b)), it is clear that the sample under nitrogen had higher BET and *t-plot* surface area, larger pore volume and micropore volume, and smaller average pore radius than the sample under air. This can be attributed to the change of pore structure and properties induced from the bulk and internal oxygen vacancies under nitrogen atmosphere [37].

Characteristic photoelectron lines can well provide information for the surface characteristics of the samples under nitrogen and air condition. Fig. 6 displays the XPS spectra of O 1s and Ti 2p lines derived from TiO_2/kaolinite composite and the corresponding fits, and Fig. S5 provided the N1s spectra information. As seen from the survey spectra, higher intensity was obtained under nitrogen condition compared with air condition, indicating the migration and movement of Ti and O atoms from the titanium array and lattice oxygen. The O 1s spectra could be fitted into three peaks (Fig. 6(b and e)). The peaks at around 529.6 and 531.0 eV are ascribed to Ti—O and surface —OH, respectively. About the peak around 532.2 eV may be related to the adsorbed H_2O [34]. The peak at around 529.6 eV had an obvious intensity increase under nitrogen atmosphere which could be attributed to the

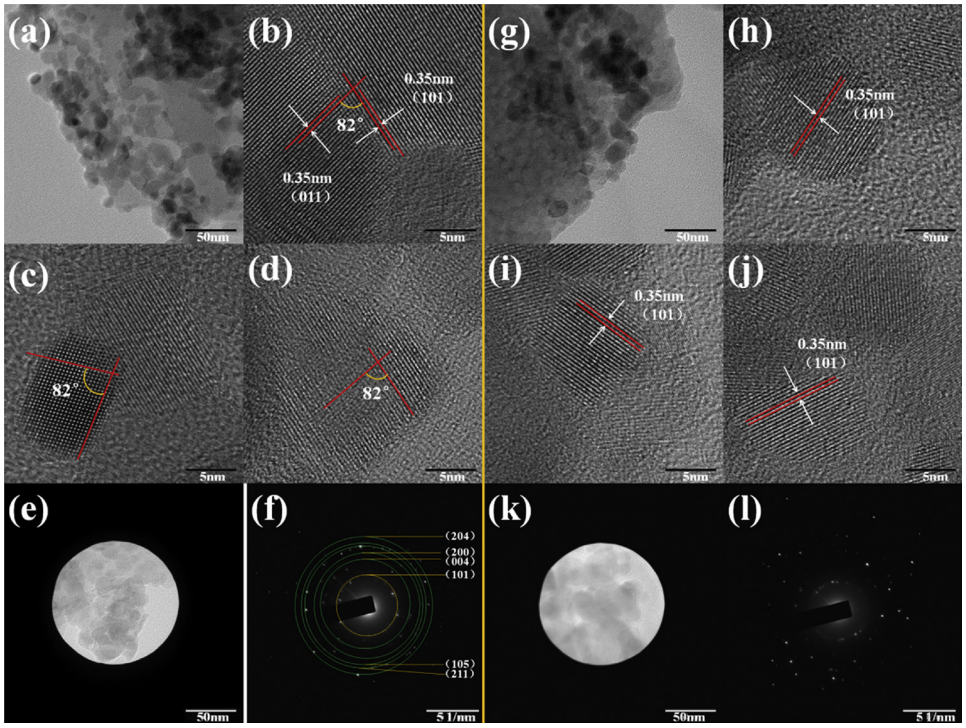

Fig. 4. HRTEM images (a–d) and SAED pattern (e and f) of TiO_2/kaolinite composites under nitrogen atmosphere (800 °C), HRTEM images (g– j) and SAED pattern (k and l) of TiO_2/kaolinite composite under air atmosphere (800 °C).

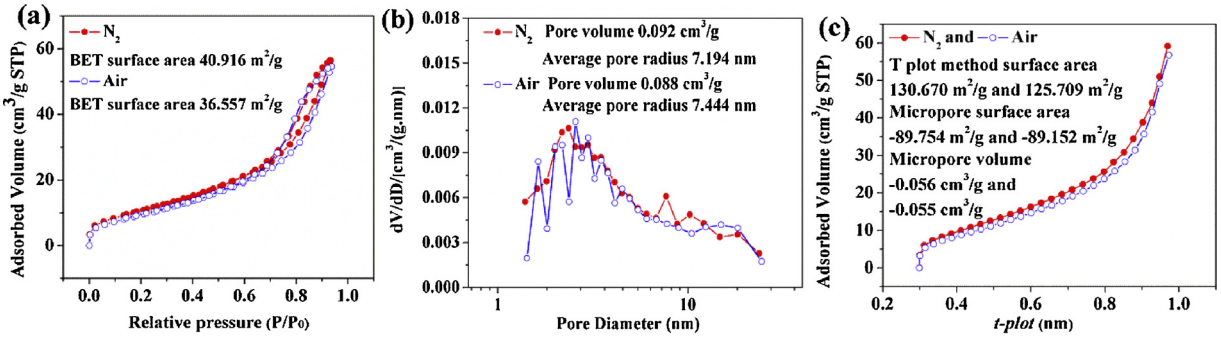

Fig. 5. (a) Nitrogen adsorption and desorption isotherms (77 K), (b) BJH pore size distribution plots and (c) *t-plot* for nitrogen absorbed at 77 K for TiO_2/kaolinite composites under nitrogen and air atmosphere (800 °C).

generation of intrinsic deficiencies and the escape of titanium element, some absorbed hydroxyl groups would tend to dehydrate to form Ti—O bonds by combining with the escaped titanium [38]. As for the Ti 2p spectra, the Ti 2p line could be mainly divided into two parts. The dominant one is consistent with the Ti 2p3/2 signal situated at around 458.5 eV, and the second contribution corresponded to the Ti 2p1/2 signal located at around 464.3 eV, both of them could be readily attributed to TiO_2. It is worth to mention that at around 460.1 eV, the signal fitted to TiO, suggesting the presence of Ti (II) oxide within the titanium dioxide because of the oxygen vacancies [39]. Considering the position of binding energy and the small content of N1s in the samples under N_2 and air condition, no lattice N (Ti—N) was formed in this work, this further demonstrated that nitrogen atmosphere played a major role in forming abundant oxygen vacancies on the surface of TiO_2/kaolinite composite rather than N element doping [40].

The prepared samples were tested by the degradation of ciprofloxacin under UV, solar, and visible light. As seen from Fig. 7, the sample employed kaolinite as the substrate exhibited high adsorption capacity compared with bare TiO_2, which are beneficial for the adsorption and degradation of the target contaminants. As for the photocatalytic activity, TiO_2/kaolinite composite obtained under nitrogen atmosphere exhibited considerably higher activity than other control samples, indicating abundant oxygen vacancies were generated on the nitrogen treated TiO_2/kaolinite surface. The nearest Ti atoms are inclined to move away from the vacancy and toward the remaining O neighbors since the oxygen vacancies are positive-charged. This will also cause the decrease of Ti—O bond length and the increase of bonding energy (Fig. 6(c and f)) [26]. Furthermore, the photocatalytic decomposition of ciprofloxacin by different samples followed pseudo first-order kinetics as shown in Fig. 7(b, d, and f). The corresponding rate constants for decomposition of CIP over the nitrogen treated TiO_2/kaolinite were 0.06144 min^{-1}, 0.00596 min^{-1} and 0.00116 min^{-1} under UV, solar and visible light, respectively. The photocatalytic degradations of nitrogen treated TiO_2/kaolinite under UV, solar and visible light were almost 7.00, 2.54 and 3.13 times, respectively, higher than those of pure TiO_2 calcined under air condition. The results

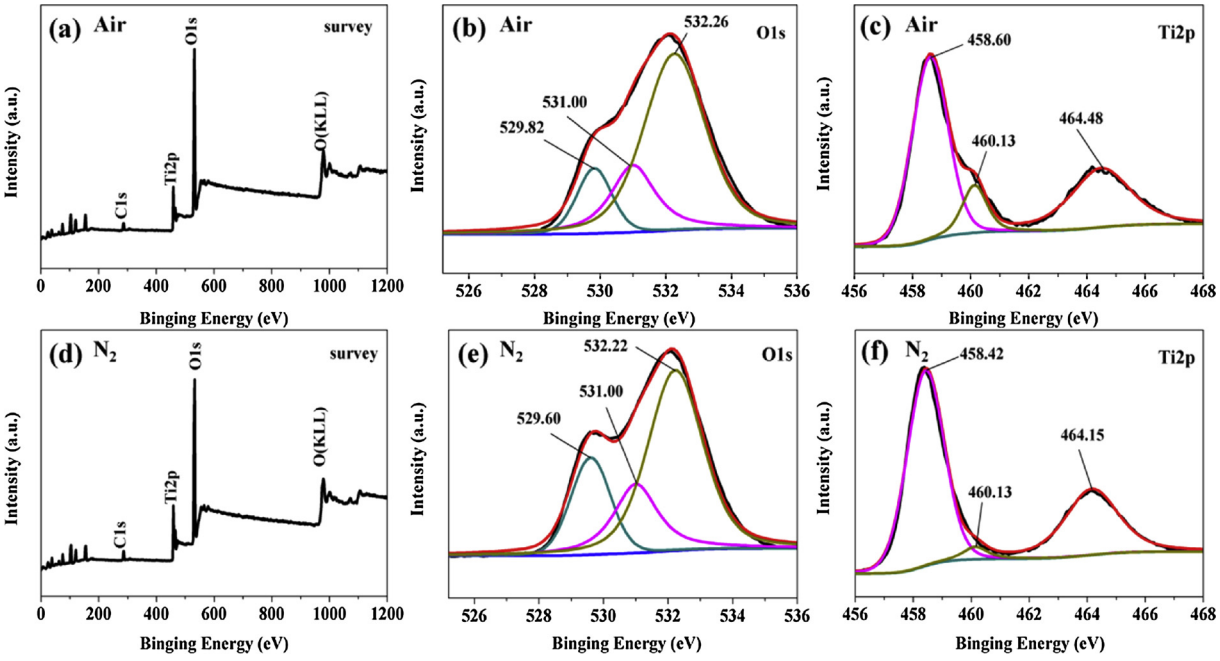

Fig. 6. (a) XPS spectra of (a and d) survey, (b and e) O1s and (c and f) Ti2p for TiO_2/kaolinite composite under nitrogen and air atmosphere (800 °C).

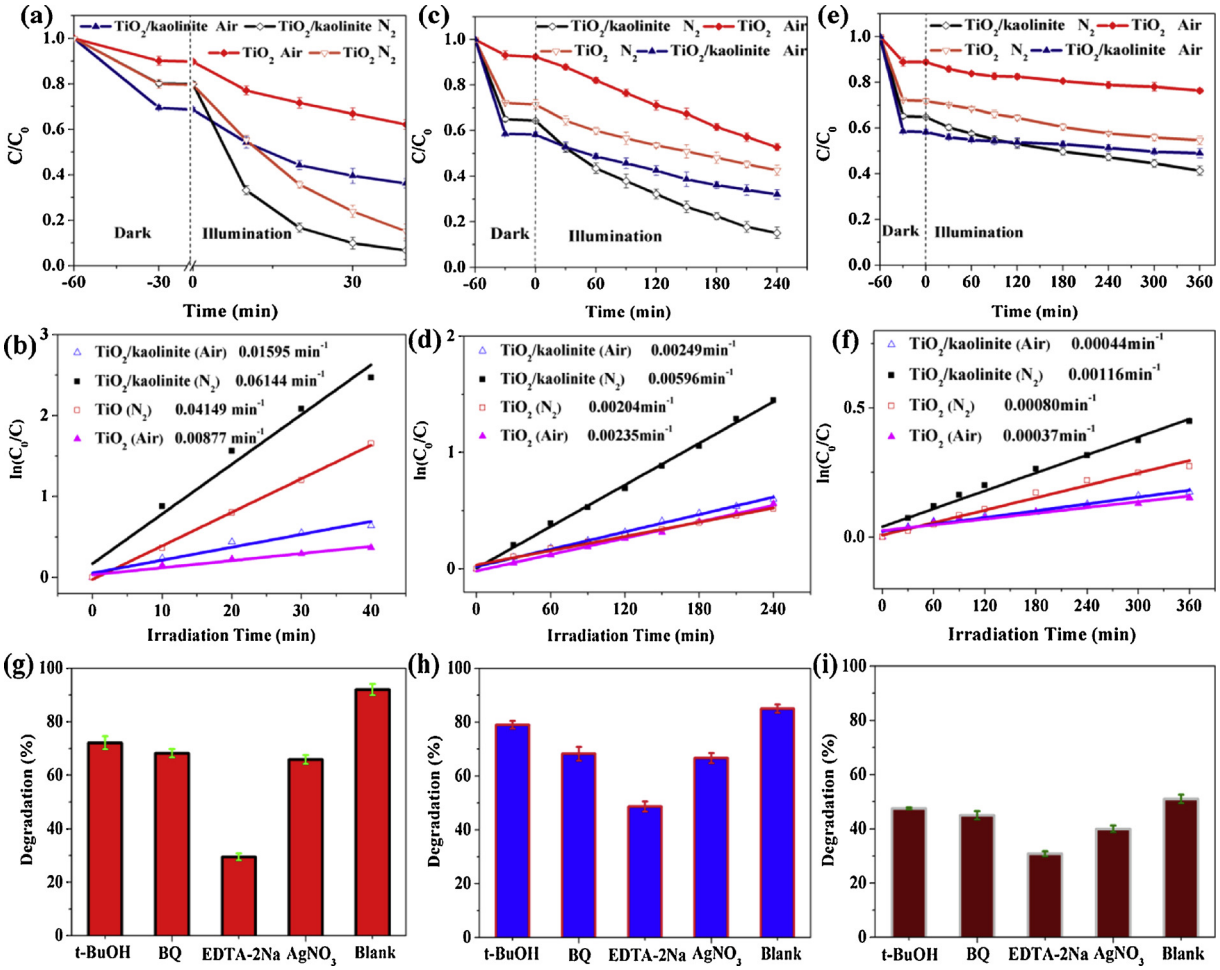

Fig. 7. Degradation of CIP under UV light (a), solar light (c) and visible light (e); First order reaction models of CIP degradation under UV light (b), solar light (d) and visible light (f); Radical scavenger experiments under UV light (g), solar light (h) and visible light (i) of TiO_2/kaolinite composites under nitrogen atmosphere (800 °C) towards CIP.

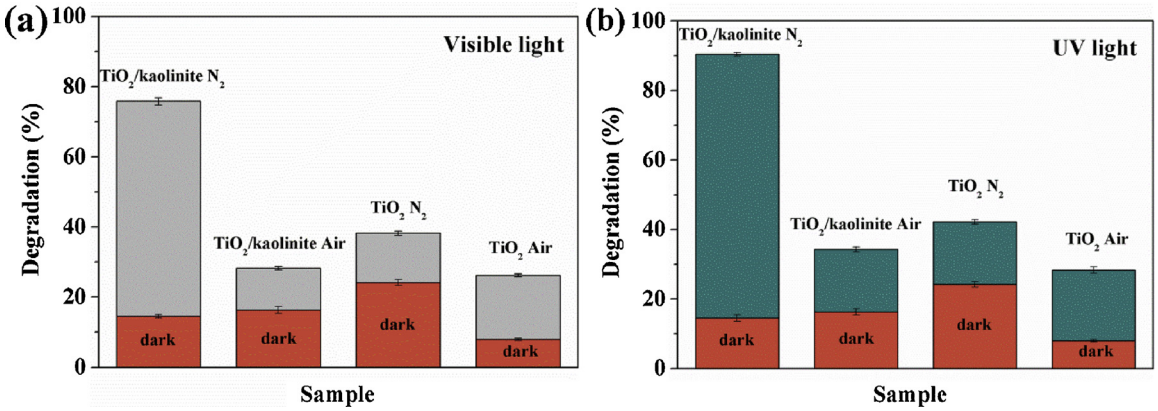

Fig. 8. Photocatalytic degradation results of formaldehyde by TiO_2/kaolinite composites under nitrogen atmosphere (800 °C) as well as the references under UV light (b) and visible light (a).

obtained in the studies of photocatalytic activity evaluation of the tested materials are consistent with the results of aforementioned material characterization analyses.

Considering the excellent degradation ability of the prepared samples towards the aqueous contaminant (CIP), a typical VOC (formaldehyde) was also introduced to examine the universality of the nitrogen treated TiO_2/kaolinite composite (Fig. 8). The samples displayed much higher elimination ability compared with the references no matter under visible light or UV light. Especially in contrast with pure TiO_2 under air condition, the ultimate removal rate of the nitrogen treated TiO_2/kaolinite composite indicated a nearly 2-fold increase towards formaldehyde within the broad spectrum, demonstrating the common activity and non-selectivity of the oxygen vacancy induced TiO_2/kaolinite composite.

In subsequent studies, 10 mM of tert butanol (t-BuOH), silver nitrate ($AgNO_3$), edentate disodium (EDTA-2Na) and 1,4-benzoquinone (BQ) were used as the scavengers of hydroxyl radical (·OH), electron (e^-), hole (h^+) and superoxide radical (·O_2^-), respectively, to elucidate the roles of different radicals in the photodegradation process (Fig. 7(g– i)) [41]. The experimental results showed that the addition of EDTA-2Na had a dominant effect on the degradation process no matter under UV light or visible light. Furthermore, in comparison with degradation reaction under visible light, the degradation for CIP was much more depressed under UV light when adding EDTA-2Na, indicating that higher percentage of holes were participated in the degradation process. It is also noticed that distinct decrease was achieved when t-BuOH, $AgNO_3$ and BQ were added, suggesting the subordinate significant roles of other radical species. This also could be verified from the ESR results as demonstrated in Fig. 9. After adding DMPO, the characteristic signals of DMPO-·OH adducts with the intensities of 1:2:2:1 and DMPO-·O_2^- adducts with six characteristic peaks were displayed. Moreover, the intensity of hole was higher than other radicals (·OH and ·O_2^-), demonstrating the dominant role of holes in the degradation process.

Photoluminescence spectra (PL) are one of the most efficient methods to examine the separation and recombination efficiency of carriers. As presented in Fig. 10(a), weaker luminous peak intensity was observed for the nitrogen treated TiO_2/kaolinite composite compared with air condition, suggesting higher percentage of charge carriers was effectively separated and transported. The electrochemical impedance spectroscopy (EIS) and transient photocurrent response were also recorded for a better understanding of carriers' separation and transfer performance (Fig. 10(b and c)). It is notable that the radius of the Nyquist circle was much smaller and the photocurrent intensity was greatly enhanced for the TiO_2/kaolinite composite under nitrogen condition, indicating the charge separation had been greatly promoted. This also confirmed that more oxygen vacancies and active catalytic sites could be beneficial for the photocatalytic performance improvement. As for the I–V curves (Fig. 10(d)), an enhanced photocurrent density was obtained for the TiO_2/kaolinite composite under nitrogen condition, which was much higher than that under air condition. This further proved the pivotal role of oxygen deficiencies in improving carrier density and electronic conductivity [42,43]. In addition, the Mott-Schottky (M-S) curves for TiO_2/kaolinite composite under nitrogen and air condition were displayed in Fig. 10(e), both of them indicated the typical n-type characteristics. Because the frequencies do not affect the intersection points, thus the flat band positions can be determined from the intersections, which are approximately −0.41 V and −0.39 V for TiO_2/kaolinite composite under nitrogen and air condition, respectively. Hence, the conduction band (CB) of TiO_2/kaolinite composite under nitrogen and air condition is estimated to be −0.41 V and −0.39 V, respectively [44]. As seen from Fig. 10(f), the band gaps can be obtained from the UV–vis curves and are determined to be 3.08 eV and 3.22 eV for TiO_2/kaolinite composite under nitrogen and air condition, respectively. Thus the corresponding valence band (VB) positions can be calculated to be 2.67 V and 2.83 V, respectively [45].

In this work, the photocatalytic enhancement mechanism for the nitrogen treated TiO_2/kaolinite composite within broad spectrum was proposed and illustrated as displayed in Scheme 3. First, natural minerals have many merits such as thermal and chemical stability and high adsorption capacity which could induce higher degradation ability compared with pure catalysts. This can be attributed to the chemically bond interfacial contact within the newly composites as well as good dispersion of nano TiO_2 on the minerals' surface with smaller grain sizes [46]. In this study, kaolinite endowed with rich negatively charge on the surface will generate strong electrostatic repulsion as well which would contribute to the photogenerated carriers' efficient space separation [25]. Based on the aforementioned characterization and analyses results obtained, the valance band (VB) and conduction band (CB) of TiO_2/kaolinite composite under air and nitrogen condition are presented in Scheme 3. Notably, lower band gap was obtained for the TiO_2/kaolinite composite under nitrogen atmosphere, which could allow utilization of the broad spectrum of sun light. The band gap energy between the oxygen vacancy states and the conduction band was determined to be 0.75–1.18 eV through measuring the energy of the ionized electrons from an oxygen vacancy in the TiO_2 single crystal [14]. The oxygen vacancy states would participate into the photo-excitation processes under illumination. Lattice oxygen deficiency in TiO_2 induced from the nitrogen would contribute to generate atomic oxygen and electrons ($O = 1/2\ O_2 + V_0^{2+} + 2e^-$); this makes the electrons

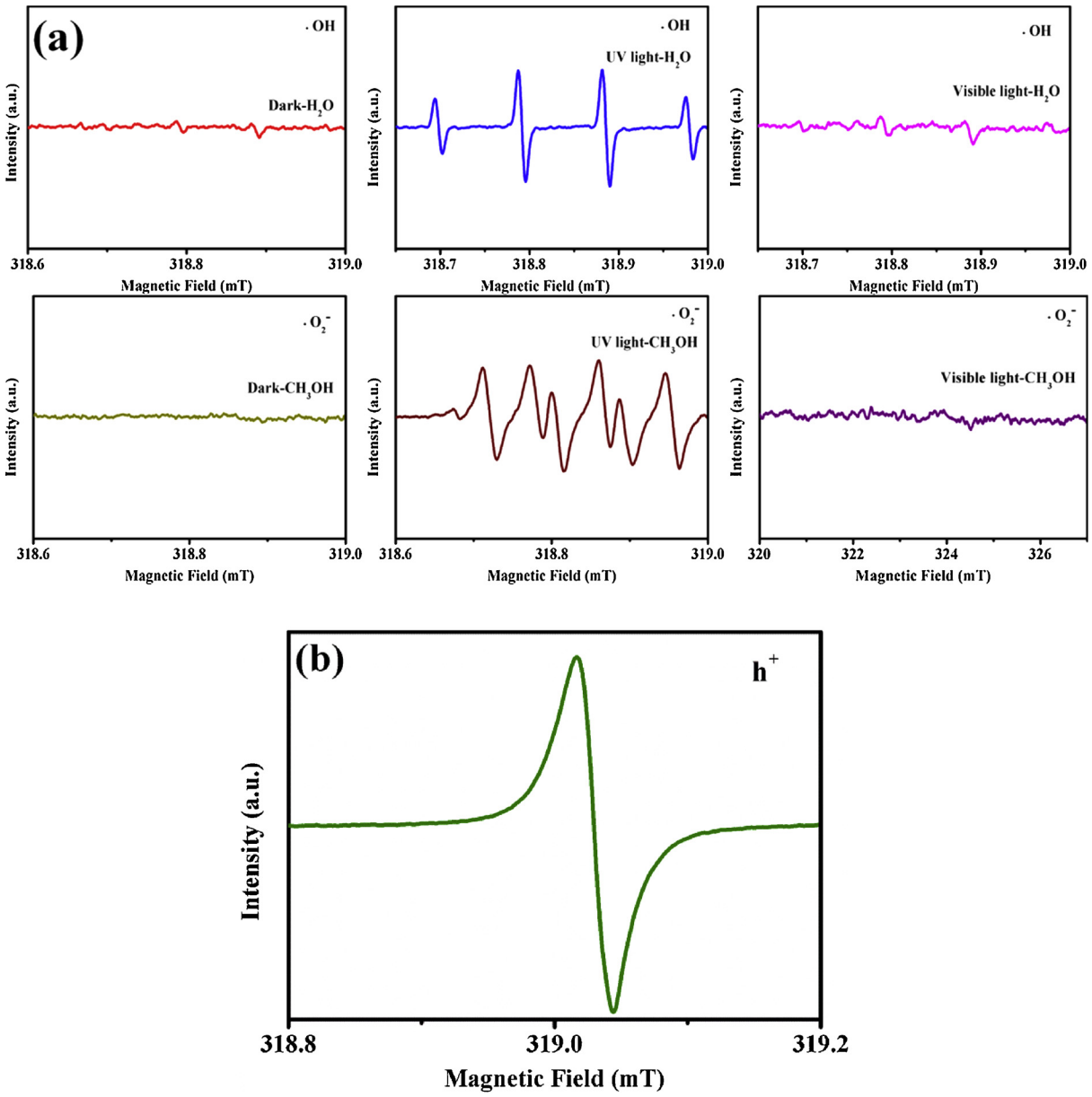

Fig. 9. (a) ESR spectra (DMPO spin-trapping) for nitrogen treated TiO_2/kaolinite composite (800 °C) under dark, UV light and visible light in aqueous for DMPO-·OH as well as CH_3OH for DMPO-·O_2^-, (b) solid ESR spectra of h^+ for nitrogen treated TiO_2/kaolinite composite (800 °C).

transition and reaction much easier considering the abundant carriers and superficial oxygen [47]. Combining with the results of ESR spectra, holes will be generated in the valance band (VB) of TiO_2 when the photocatalysts are under illumination, and the photogenerated electrons will transfer to the conduction band (CB). The photogenerated electrons could produce ·O_2^- through reduction of the absorbed O_2; this can be attributed to the position of CB of TiO_2 which is lower than the O_2/·O_2^- potential. In addition, due to the oxygen vacancy intermediate level, the absorbed O_2 would react with electrons form H_2O_2 ($O_2 + 2H^+ + 2e^- \rightarrow H_2O_2$; ·$O_2^- + 2H^+ + e^- \rightarrow H_2O_2$) and then transformed into ·OH by further reacting with the electrons and water molecules. Based on the relative intensity of carriers involved in the reaction, holes should be the main oxidizing species within broad spectrum, and ·OH, ·O_2^- and e^- are also playing significant role in the photocatalytic process. Therefore, the synergistic effect between the constructed 0D/2D structure and the oxygen vacancies confined in the interfacial assembly promote the superior degradation towards ciprofloxacin (i.e., one of PPCPs) and formaldehyde (i.e., one of VOCs). Due to the presence of mid-state, much more photons can be excited and separated due to the lower band level, thus quantum efficiency will be improved in the degradation process. In conclusion, the high degradation within broad spectrum is attributed to the formation of oxygen vacancy intermediate level, the reduction of the band gap energy, and the increased light absorption and carriers' separation efficiency.

4. Conclusions

In summary, a novel 0D/2D TiO_2/kaolinite composite endowed with oxygen vacancy state and surface defect sites was facilely prepared via a mild sol-gel method combining with nitrogen atmosphere induction in this work. The crystallographic, morphological, valence bonding and states, optical and other characterizations demonstrated the

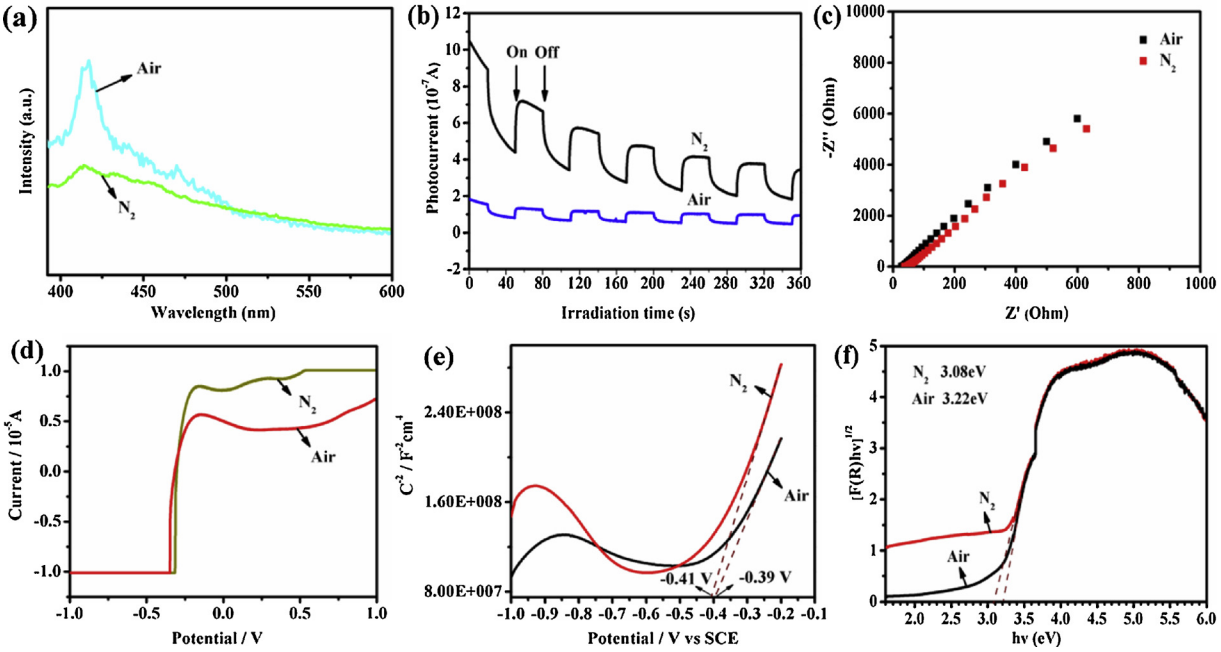

Fig. 10. (a) PL spectra, (b) photocurrent, (c) EIS plots, (d) I–V curves, (e) Mott-Schottky plots and (f) band gaps of TiO_2/kaolinite composite under air and nitrogen atmosphere (800 °C).

generation of oxygen vacancy state within the newly prepared nitrogen treated TiO_2/kaolinite composite, which contributed the enhancement of degradation activity within broad spectrum radiation. Furthermore, better dispersion and smaller grain sizes of nano TiO_2 on the surface of kaolinite, enlarged surface area, and strong electrostatic repulsion play a pivotal role in the enhancement mechanism as well. The as-synthesized nitrogen treated TiO_2/kaolinite composite presented good photocatalytic degradation towards CIP under broad spectrum illumination, the reaction rate constant of which is almost 7.00, 2.54 and 3.13 times higher than that of pure TiO_2 treated with air under UV, solar and visible light, respectively. Besides, the as-prepared composite also exhibited better formaldehyde removal performance in comparison with other samples in this study; a nearly 2-fold increase towards formaldehyde degradation under broad spectrum illumination in comparison with pure TiO_2 treated with air was achieved. Based on radical scavenger experiments and ESR testing, holes are the main oxidizing species within broad spectrum illumination. The present study can provide new insight into the preparation of highly-efficient composite photocatalysts based on minerals within broad spectrum illumination, which exhibit potential industrial application in the fields of PPCPs and VOCs degradation.

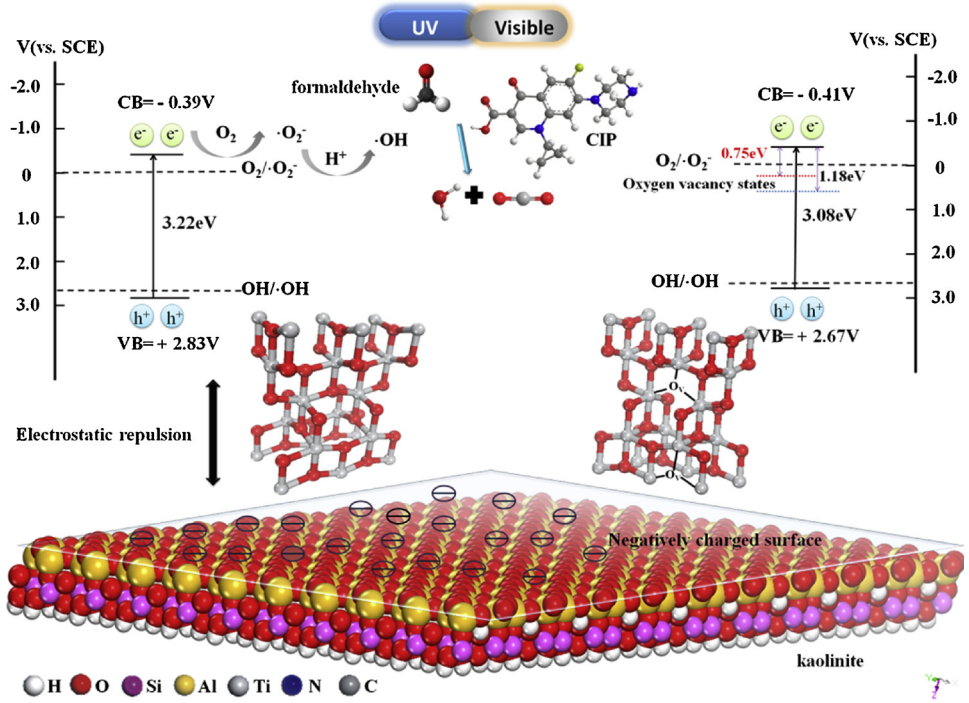

Scheme 3. The diagram description of the photocatalytic degradation enhancement mechanism of the nitrogen treated TiO_2/kaolinite composite.

Acknowledgments

The authors gratefully acknowledge the financial support provided by the National Key R&D Program of China (2017YFB0310803-4), the National Natural Science Foundation of China (Grant No. 51504263) and the Fundamental Research Funds for the Central Universities (2015QH01 and 2010YH10). The first author also thanks the China Scholarship Council (CSC) for financial support.

Appendix A. Supplementary data

Supplementary material related to this article can be found, in the online version, at doi:https://doi.org/10.1016/j.apcatb.2018.04.083.

References

[1] E.N. Evgenidou, I.K. Konstantinou, D.A. Lambropoulou, Sci. Total Environ. 505 (2015) 905–926.
[2] J. Wang, S. Wang, J. Environ. Manage. 182 (2016) 620–640.
[3] Y.S. Son, Chem. Eng. J. 316 (2017) 609–622.
[4] R. Pal, K.H. Kim, Y.J. Hong, E.C. Jeon, J. Hazard. Mater. 153 (2008) 1122–1135.
[5] M.D. Hernándezalonso, F. Fresno, S. Suárez, J.M. Coronado, Energy Environ. Sci. 2 (2009) 1231–1257.
[6] X. Wu, M. Li, J. Li, G. Zhang, S. Yin, Appl. Catal. B: Environ. 219 (2017) 132–141.
[7] Vaidyanathan Subramanian, Eduardo Wolf, P.V. Kamat, J. Phys. Chem. B 105 (2011) 11439–11446.
[8] X.C. And, C. Burda, J. Phys. Chem. B 108 (2004) 15446–15449.
[9] H. Li, Z. Bian, J. Zhu, Y. Huo, H. Li, Y. Lu, J. Am. Chem. Soc. 129 (2007) 4538–4539.
[10] C. Li, Z. Sun, Y. Xue, G. Yao, S. Zheng, Adv. Powder Technol. 27 (2016) 330–337.
[11] X. Chen, L. Liu, P.Y. Yu, S.S. Mao, Science 331 (2011) 746–750.
[12] X. Chen, S.S. Mao, ChemInform 107 (2007) 2891–2959.
[13] A. Naldoni, M. Allieta, S. Santangelo, M. Marelli, F. Fabbri, S. Cappelli, C.L. Bianchi, R. Psaro, S.V. Dal, J. Am. Chem. Soc. 134 (2012) 7600–7603.
[14] X. Pan, M.Q. Yang, X. Fu, N. Zhang, Y.J. Xu, Nanoscale 5 (2013) 3601–3614.
[15] S. Mansingh, D.K. Padhi, K.M. Parida, Catal. Sci. Technol. 7 (2017) 2772–2781.
[16] T.L. Thompson, Y.J. Jr, Chem. Rev. 106 (2006) 4428–4453.
[17] H. Li, J. Shang, Z. Ai, L. Zhang, J. Am. Chem. Soc. 137 (2015) 6393–6399.
[18] G. Zhang, X. Ding, Y. Hu, B. Huang, X. Zhang, X. Qin, J. Zhou, J. Xie, J. Phys. Chem. C 112 (2015) 17994–17997.
[19] S. Fukahori, H. Ichiura, T. Kitaoka, H. Tanaka, Environ. Sci. Technol. 37 (2003) 1048–1051.
[20] B. Wang, G. Zhang, L. Xue, Z. Sun, S. Zheng, J. Hazard. Mater. 285 (2015) 212–220.
[21] Y. Zhang, H. Gan, G. Zhang, Chem. Eng. J. 172 (2011) 936–943.
[22] V.D. Mote, Y. Purushotham, B.N. Dole, J. Theor. Appl. Phys. 6 (2012) 6–13.
[23] G. Zhang, Z. Sun, Y. Duan, R. Ma, S. Zheng, Appl. Surf. Sci. 412 (2017) 105–112.
[24] C. Li, Z. Sun, L. Liu, W. Huang, S. Zheng, RSC Adv. 6 (2016) 91002–91011.
[25] C. Li, Z. Sun, W. Huang, S. Zheng, J. Taiwan Inst. Chem. Eng. 66 (2016) 363–371.
[26] S. Wang, L. Zhao, L. Bai, J. Yan, Q. Jiang, J. Lian, J. Mater. Chem. A 2 (2014) 7439–7445.
[27] W.T. Yao, S.H. Yu, Q.S. Wu, Adv. Funct. Mater. 17 (2010) 623–631.
[28] T. Ohsaka, J. Phys. Soc. Jpn. 48 (2007) 1661–1668.
[29] S. Sahoo, A.K. Arora, V. Sridharan, J. Phys. Chem. C 113 (2017) 16927–16933.
[30] C. Han, E. Sahle-Demessie, A. Shah, S. Nawaz, Latif-ur-Rahman, N.B. Mcguinness, S.C. Pillai, H. Choi, D.D. Dionysiou, M.N. Nadagouda, Room Temperature Catalysis for Environmental Applications vol. 8, (2018), pp. 207–230.
[31] M. Lohrasbi, ACS Appl. Mater. Interfaces 6 (2014) 2692–2699.
[32] F. Lei, Y. Sun, K. Liu, S. Gao, L. Liang, B. Pan, Y. Xie, J. Am. Chem. Soc. 136 (2014) 6826–6829.
[33] C. Li, Z. Sun, R. Ma, Y. Xue, S. Zheng, Microporous Mesoporous Mater. 243 (2017) 281–290.
[34] L. Deng, Y. Xie, G. Zhang, Chin. J. Catal. 38 (2017) 379–388.
[35] H. Xu, P. Reunchan, S. Ouyang, H. Tong, N. Umezawa, T. Kako, J. Ye, Chem. Mater. 25 (2013) 405–411.
[36] W. Qian, P.A. Greaney, S. Fowler, S.K. Chiu, A.M. Goforth, J. Jiao, ACS Sustain. Chem. Eng. 2 (2014) 1802–1810.
[37] A. Galarneau, F. Villemot, J. Rodriguez, F. Fajula, B. Coasne, Langmuir 30 (2014) 13266–13274.
[38] J. Yu, G. Wang, B. Cheng, M. Zhou, Appl. Catal. B: Environ. 69 (2007) 171–180.
[39] K. Batalović, N. Bundaleski, J. Radaković, N. Abazović, M. Mitrić, R.A. Silva, M. Savić, J. Belošević-Čavor, Z. Rakočević, C.M. Rangel, Phys. Chem. Chem. Phys. PCCP 19 (2017) 7062–7071.
[40] H. Xu, L. Zhang, J. Phys. Chem. C 114 (2010) 11534–11541.
[41] C. Li, Z. Sun, W. Zhang, C. Yu, S. Zheng, Appl. Catal. B: Environ. 220 (2018) 272–282.
[42] J. Cao, Y. Zhang, H. Tong, P. Li, T. Kako, J. Ye, Chem. Commun. 48 (2012) 8649–8651.
[43] H. Xu, S. Ouyang, L. Liu, P. Reunchan, N. Umezawa, J. Ye, J. Mater. Chem. A 2 (2014) 12642–12661.
[44] Q. Liang, M. Zhang, C. Liu, S. Xu, Z. Li, Appl. Catal. A: Gen. 519 (2016) 107–115.
[45] J. Jiang, L. Zhang, H. Li, W. He, J.J. Yin, Nanoscale 5 (2013) 10573–10581.
[46] Z. Sun, C. Li, G. Yao, S. Zheng, Mater. Des. 94 (2016) 403–409.
[47] I. Nakamura, N. Negishi, S. Kutsuna, T. Ihara, S. Sugihara, K. Takeuchi, J. Mol. Catal. A: Chem. 161 (2000) 205–212.